PASJ: Publ. Astron. Soc. Japan **57**, 259–271, 2005 February 25

Gigabit Digital Filter Bank: Digital Backend Subsystem in the VERA Data-Acquisition System

Satoru IGUCHI,[1] Tomoharu KURAYAMA,[1,2] Noriyuki KAWAGUCHI,[1] and Kazuyuki KAWAKAMI[3]
[1]*National Astronomical Observatory, 2-21-1 Osawa, Mitaka, Tokyo 181-8588*
s.iguchi@nao.ac.jp
[2]*Department of Astronomy, School of Science, The University of Tokyo, Hongo, Tokyo 113-0033*
[3]*Elecs Industry CO., LTD, 1-22-23 Sinsaku, Takatu, Kawasaki 213-0014*

(Received 2004 October 18; accepted 2004 December 22)

Abstract

The VERA terminal is a new data-acquisition system developed for the VERA project, which is a project to construct a new Japanese VLBI array dedicated to make a 3-D map of our Milky Way Galaxy in terms of high-precision astrometry. New technology, a gigabit digital filter, was introduced in the development. The importance and advantages of a digital filter for radio astronomy have been studied as follows: (1) the digital filter can realize a variety of observation modes and maintain compatibility with different data-acquisition systems (Kiuchi et al. 1997 and Iguchi et al. 2000a), (2) the folding noise occurring in the sampling process can be reduced by combination with a higher-order sampling technique (Iguchi, Kawaguchi 2002), (3) and an ideal sharp cut-off bandedge and a flat amplitude/phase responses are approached by using a large number of taps available to use LSI of a large number of logic cells (Iguchi et al. 2000a). We developed the custom Finite Impulse Response filter chips and manufactured the Gigabit Digital Filter Banks (GDFBs) as a digital backend subsystem in the VERA terminal. In this paper, the design and development of the GDFB are presented in detail, and the performances and demonstrations of the developed GDFB are shown.

Key words: instrumentation: interferometers — radio continuum: general — radio lines: general — reference systems — techniques: high resolution

1. Introduction

In radio astronomical observations, two completely different types of signals from celestial objects are observed with a radio telescope. One is continuum emission over a wide range of frequencies, resulting from blackbody or synchrotron radiation, and another is line emissions arising from molecular/atomic/ionic species. Sometimes the line emission source emits signals in two widely separated frequency regions originated in a high speed rotating gas around a massive core. For a continuum emission source, the full range of the receiver band is processed with a limited frequency resolution, but for a line emission source the specific frequency region should be processed with much higher frequency resolution. For the latter case, an analog bandpass filter of fixed bandwidth on a fixed central frequency has been used so far. Frequency tuning of the spectral line emission inside the narrow band filter has been made by changing the frequency of a local oscillator in the receiver. However, in the case that there are several line emission sources within the frequency coverage of the receiver, it is difficult to receive them simultaneously with the analog filter. The receiver used in radio interferometry is capable of receiving a wide frequency range of typically more than 1 GHz. A digital filter of having a processing speed of 1 Gbit per second or higher offers a perfect solution for these radio astronomical observations, because some frequency bands can be arbitrary cut with the digital filter.

VERA (VLBI Exploration of Radio Astrometry) is a project to construct a new Japanese VLBI system (Very-Long-Baseline Interferometry) dedicated to differential VLBI in order to measure the position and proper motion of the galactic masers with 10 microarcsec level accuracy (e.g. Sasao 1996; Honma et al. 2000). The VERA's radio telescopes have a fully steerable dual-beam system with which we can observe two adjacent sources simultaneously by moving the steerable receivers with a Stewart platform (Kawaguchi et al. 2000). By removing the atmospheric fluctuation effectively based on a dual-beam observation, the VERA can measure the position of galactic maser relative to an extra-galactic reference source with unprecedentedly high accuracy (Kobayashi et al. 2003). For the realization of simultaneously observing both a galactic maser and an extra-galactic source, GDFBs (Gigabit Digital Filter Banks) were implemented as a digital backend subsystem in the data-acquisition system newly developed for VERA, the VERA terminal.

This paper presents the first astronomical capability and performances of our developed GDFB. An outline of this paper is as follows: section 2 shows the requirements and specifications of the VERA digital backend subsystem, the GDFB; section 3 presents the design and development of the GDFB; section 4 shows the digital filtering performances and astronomical demonstrations of the GDFB; and finally section 5 provides the summary of this paper.

2. Principles of Gigabit Digital Filter Bank Design

Two 2-bit Analog-to-Digital Converters (ADCs) working at an 1-GHz sampling rate have been introduced for a

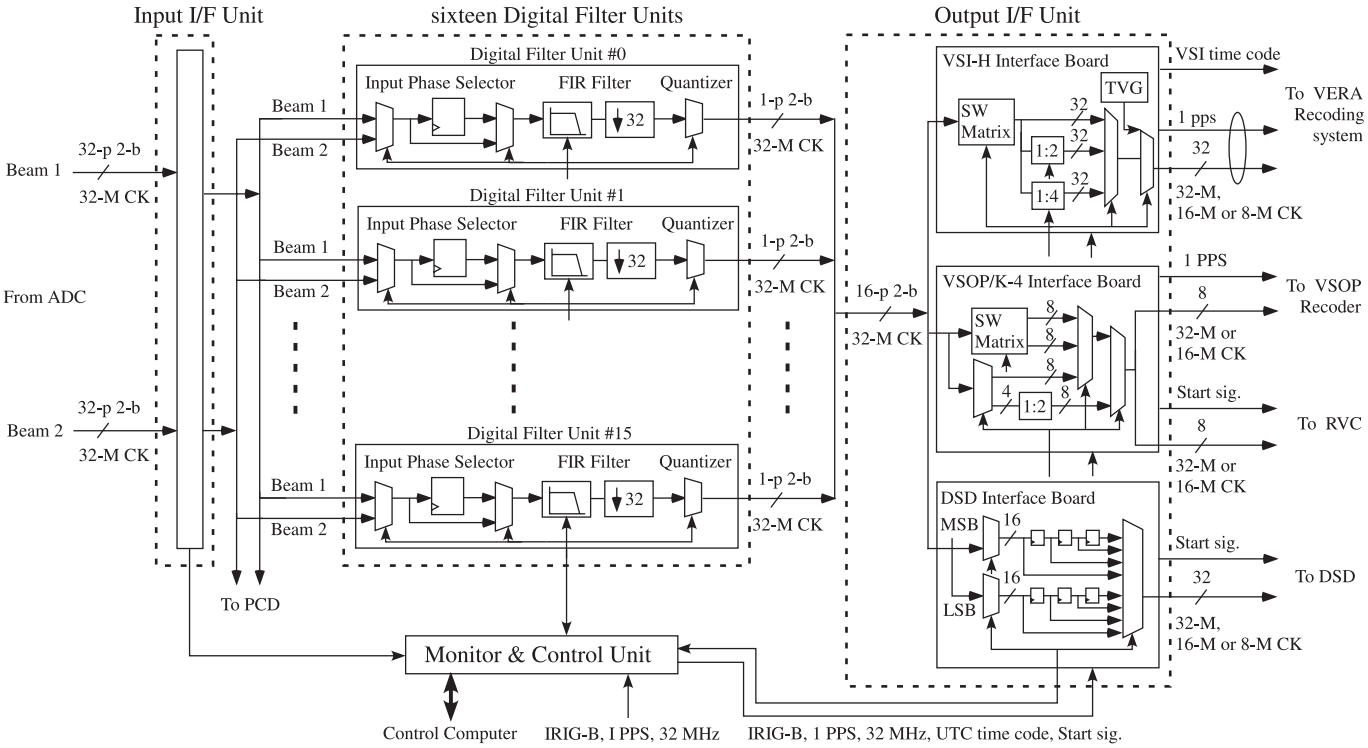

Fig. 1. Block diagram of Gigabit Digital Filter Bank (GDFB). The GDFB consists of Input I/F Unit, sixteen Digital Filter Units, Output I/F Unit, and Monitor and Control Unit. The Input I/F Unit converts ECL (Emitter Coupled Logic) to TTL (Transistor–Transistor Logic), and measures the bit distribution of the input signal from each ADC. The sixteen Digital Filter Units select the input signals from each beam, and cut the requested bandwidth in the frequency range of 512 MHz. Since the decimation factor at the Digital Filter Units is fixed at 32, its output is an 1-parallel 2-bit 32-MHz clock. Each Digital Filter Unit has the function of bit distribution measurement for the output signals after digital filtering. The GDFB supports the VLBI Hardware Standard Interface (VSI-H)[1] and can directly connect the VSI-H Data Input Module at hardware interface. The Output I/F Unit is connected to the VERA recording system conformable to the VSI-H, the VSOP recorder to join the VSOP observation (Iguchi et al. 2000a) and for K-4 recording (Kiuchi et al. 1997), and the Realtime VLBI Correlator (RVC, Iguchi et al. 2000b) and the Digital Spectral Detector (DSD) modifying for the VERA [from digital spectrometer developed in Sorai et al. (2000)] to check at realtime the digital spectrum of the observation data that is directly recorded at the VERA recorder. The circle of 1 PPS and Data streams from the VSI-H interface board means transmission on the same cable. The Test Vector Generator (TVG) data streams are defined by the VSI-H, and this TVG is effective to check the internal self-contained diagnostics and the bit error, and to confirm the external interface connectivity to the recorders. The 8-MHz bandwidth is realized by choosing one sample every two in the Output I/F Unit. The Phase Calibration Detector (PCD), which is also made by improving the input board of DSD, is used to calibrate the relative phase fluctuation of different transmission paths between Beam 1 and 2. The Monitor and Control Unit sets up the parameters corresponding to each unit by the observation mode, synchronizes the data with the time, and monitors the setting parameters and the status. The VSI time code (VERA specific) is generated in the VSI-H interface board from IRIG-B signal, 1 PPS and 32-MHz clock. Since an internal clock generator is introduced in the Monitor and Control Unit, it is also possible to control the time, even if it does not receive the IRIG-B signal, 1 PPS and 32-MHz clock.

dual-beam system in the VERA radio telescope. The ADCs were fabricated by improving a digital oscilloscope made by Sony/Tektronix Company (as developed in the BEARS project: Sunada et al. 2000). However, the digital oscilloscope is presently discontinued. The ADS-1000, made by Digital Link Company, will replace it as the next-generation VERA ADC at an early date. In other data-acquisition systems, the current standard bandwidth is 8 or 16 MHz in astronomically observing, while the maximum number of IF is 16 channels (Iguchi et al. 2000a; Kiuchi et al. 1997; Napier et al. 1994; Whitney 1993). The bandwidth compatibility with the other data-acquisition systems is of significance in realizing global VLBI observations. Thus, the VERA terminal has the requirement that the GDFB can cut an 8-MHz bandwidth out of the range of 512 MHz.

For radio interferometry, the use of digital rather than analog instrumentation to introduce the compensating time delays, and to measure correlation has important practical advantages. For continuum emission sources, one bit per sample or two bits per sample is simple to implement, and is almost optimum in the sense that the Signal-to-Noise Ratio (*SNR*) is maximized for a limited transmission rate of the IF signals in connected radio interferometry and a fixed number of bits recorded in VLBI (Thompson et al. 2001).

The VERA terminal has digital processing, which consists of two 2-bit ADCs at a fixed sampling frequency of 1024 MHz: the GDFB with sixteen Digital Filter Units, and the VERA recorder with the maximum recording rate of 1024 Mbps (figure 1). The Digital Filter Unit should be designed at a decimation factor of 32 (= 1024 Mbps/16 ch/2 bit) to maximize the performance over saving the material cost from the viewpoint of keeping the compatibility with the other VLBI

[1] ⟨http://web.haystack.edu/vsi/index.html⟩.

Table 1. Observation modes with the VERA terminal.

Mode		Bandwidth	Number of bit	Number of channel	Recorder	Recording rate
VERA 1	Beam 1	128 MHz	2 bit	1 ch	VERA	1024 Mbps
	Beam 2	128 MHz	2 bit	1 ch		
VERA 2	Beam 1	64 MHz	2 bit	1 ch	VERA	1024 Mbps
	Beam 2	64 MHz	2 bit	3 ch		
VERA 3	Beam 1	64 MHz	2 bit	1 ch	VERA	1024 Mbps
	Beam 2	64 MHz	2 bit	1 ch		
	Beam 2	128 MHz	2 bit	1 ch		
VERA 4	Beam 1	32 MHz	2 bit	1 ch	VERA	1024 Mbps
	Beam 2	32 MHz	2 bit	7 ch		
VERA 5	Beam 1	32 MHz	2 bit	1 ch	VERA	1024 Mbps
	Beam 2	32 MHz	2 bit	1 ch		
	Beam 2	64 MHz	2 bit	1 ch		
	Beam 2	128 MHz	2 bit	1 ch		
VERA 6	Beam 1	32 MHz	2 bit	1 ch	VERA	1024 Mbps
	Beam 2	32 MHz	2 bit	3 ch		
	Beam 2	128 MHz	2 bit	1 ch		
VERA 7	Beam 1	16 MHz	2 bit	1 ch	VERA	1024 Mbps
	Beam 2	16 MHz	2 bit	15 ch		
VERA 8	Beam 1	16 MHz	2 bit	1 ch	VERA	1024 Mbps
	Beam 2	16 MHz	2 bit	1 ch		
	Beam 2	32 MHz	2 bit	3 ch		
	Beam 2	128 MHz	2 bit	1 ch		
VERA 9	Beam 1	16 MHz	2 bit	2 ch	VERA	256 Mbps
	Beam 2	16 MHz	2 bit	2 ch		
VERA 10	Beam 1	16 MHz	2 bit	8 ch	VERA	256 Mbps
	Beam 2	16 MHz	2 bit	8 ch		
Geo. 1		16 MHz	2 bit	16 ch	VERA	1024 Mbps
Geo. 2		16 MHz	1 bit	16 ch	VERA	512 Mbps
Geo. 3		8 MHz	2 bit	16 ch	VERA	512 Mbps
Geo. 4		8 MHz	1 bit	16 ch	VERA	256 Mbps
VLBI 1		256 MHz	2 bit	1 ch	VERA	1024 Mbps
VLBI 2		128 MHz	2 bit	1 ch	VERA	512 Mbps
VLBI 3		64 MHz	2 bit	1 ch	VERA	256 Mbps
VSOP 1		32 MHz	2 bit	2 ch	VSOP	256 Mbps
VSOP 2		16 MHz	2 bit	2 ch	VSOP	128 Mbps
K4		8 MHz	1 bit	16 ch	VSOP	256 Mbps

data-acquisition systems, because the material size strongly depends on the number of IF channels. In that case, the standard bandwidth becomes 16 MHz (= 512 MHz/32). In addition, sixteen 8-MHz channels of 1- or 2-bit quantization can be realized by one sample every two samples in the Output I/F Unit.

From the capability of the VERA recorder, the widest bandwidth becomes 256 MHz at 2-bit requantization after digital filtering. Defining that the total number of output channels is CH, and the bandwidth and the up-sampling at each output channel are B_i and M_i, respectively, we can derive the following relations:

$$B_i = M_i * 16\,\mathrm{MHz}, \tag{1}$$

$$\sum_{i}^{CH} B_i = 256\,\mathrm{MHz}, \tag{2}$$

where the suffix "i" is a number of the output channels and M_i is an integer. Since there are sixteen Digital Filter Units, we can also derive the five kinds of up-sampling as

$$M_i = \{1, 2, 4, 8, 16\}. \tag{3}$$

By flexibly adjusting the value of each M_i, from equations (1) and (3), the following kinds of bandwidth are realized:

$$B_i = \{16, 32, 64, 128, 256\}. \tag{4}$$

Table 2. The relationship between the input phase (Φ_I), the output phase (Φ_O), and the output bandwidth (B_i) at the observation mode of VERA 5.

	Input phase selector		Digital filter units	
Unit number	Selection beam	Input phase Φ_I	Output bandwidth B_i	Output phase Φ_O
1	Beam 1	0	32 MHz	0
2		16		1
3	Beam 2	0	32 MHz	0
4		16		1
5	Beam 2	0	64 MHz	0
6		8		1
7		16		2
8		24		3
9	Beam 2	0	128 MHz	0
10		4		1
11		8		2
12		12		3
13		16		4
14		20		5
15		24		6
16		28		7

For instance, if M_i = const., we can achieve the following observation modes: sixteen 16-MHz channels of 2-bit quantization, eight 32-MHz channels of 2-bit quantization, four 64-MHz channels of 2-bit quantization, two 128-MHz channels of 2-bit quantization, and one 256-MHz channels of 2-bit quantization. All observation modes with the VERA terminal are listed in table 1. The recording rate is always reduced in the case of an 8-MHz bandwidth or 1-bit quantization, which are effective for global geometrical observations.

All observation modes can be realized by well controlling the tap coefficients of the FIR (Finite Impulse Response) filter and the sample phase shift of the Input Phase Selector, which have a role of keeping the consistency between the sixteen Digital Filter Units (see figure 1). Defined that the input phase in the Input Phase Selector is Φ_I, the output phase after digital filtering is written as

$$\Phi_O = \frac{\Phi_I}{32} * \frac{B_i(\mathrm{MHz})}{16(\mathrm{MHz})}, \tag{5}$$

where 32 is the decimation factor in the sixteen Digital Filter Units; then, its minimum bandwidth is 16 MHz. The various bandwidths can be realized by well adjusting the input phase under the condition that the output phases from the corresponding Digital Filter Units are continuously time-series (0, 1, ...). For example, in case of the observation mode of VERA 5, the relationship between the input phase, the output phase, and the output bandwidth is given in table 2. It is understood that the Input Phase Selector does not only select the signals from each beam but also realizes more than a 16-MHz bandwidth by well adjusting the input phase.

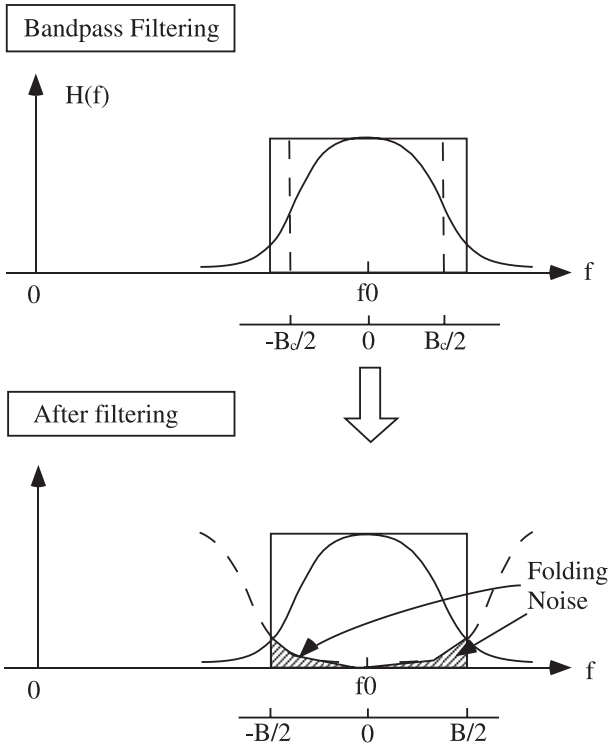

Fig. 2. Frequency response, $H(f)$, of the digital filter. It is obvious that the effect of the aliasing, the folding noise, decreases as the cut-off frequency (B_c) of the filter becomes narrower than the bandwidth (B), whereas it increases as the cut-off frequency becomes higher than the bandedge. It is also known that the non-rectangular response provides an increase in the statistical independence between samples.

The other data-acquisition systems have several IF down converters (Kiuchi et al. 1997; Napier et al. 1994; Whitney 1993), so that one can tune the IF frequency independently for all IFs, and also select Upper- or Lower-sidebands. However, the GDFB does not have a tunable digital filter function. When the VERA participates in a global VLBI observation, the other VLBI networks need to adapt the IF frequency and sideband selection to respond to a VERA observation mode.

3. Detailed Design and Development of GDFB

By limiting the tap length in the FIR filter, it is impossible to realize a filter with a perfectly rectangular bandpass response (figure 2). The FIR filtering system is written as

$$t(n) = \sum_{i=0}^{K-1} h(i) * s(n-i), \tag{6}$$

where s is the digital waveforms from the astronomical radio signals, which obeys the zero-mean Gaussian random variable; t is the output signals from FIR filter; and h is the FIR filter function with a tap length of K. The material size of the FIR filter directly depends on the tap length and the tap-coefficient word length. In developing the FIR filter, it is important to define these parameters. In subsection 3.1 these estimations are derived; the logic of the FIR filter is described in subsection 3.2; subsection 3.3 presents the custom FIR filter chip and

the Digital Filter Unit board; and finally subsection 3.4 shows the GDFB.

3.1. Tap Length and the Tap-Coefficient Word Length

It was confirmed that the folding noise is decreased by the phase-rotation stopping technique in the VLBI correlation process designed to correct a different Doppler shift in frequency at two antennas by the earth rotation (Iguchi et al. 2000a). By considering the correlation process in radio interferometry, the sensitivity loss factor due to an imperfect bandpass is derived as [see equation (2) in Iguchi, Kawaguchi (2002)],

$$\xi = \frac{\displaystyle\int_{f_0-B/2}^{f_0+B/2} H_x(f)H_y^*(f)\,df}{B} \times \frac{1}{\sqrt{1+2\displaystyle\sum_{\tau=1}^{N-1}\frac{N-\tau}{N}\frac{R_{xx}(\tau)R_{yy}(\tau)}{R_{xx}(0)R_{yy}(0)}}}, \quad (7)$$

where B is the bandwidth after filtering, N is the number of samples existing in the integration period, $H_x(f)$ and $H_y(f)$ are the frequency response of the bandpass filter, and R_{xx} and R_{yy} are the autocorrelation functions of x and y (they are the output signals of two telescopes). Because the digital-filter technique can realize stable bandpass frequency responses, the relation $H_x(f) = H_y(f) = H(f)$ is derived. The signal that is received through each telescope is written as follows; $x(n) = C_x \cdot t(n)$ and $y(n) = C_y \cdot t(n)$, where C is the constant factor estimated from effective sensitivity at each telescope. When $C_x = C_y$, equation (7) is simply replaced as

$$\xi = \frac{\displaystyle\int_{f_0-B/2}^{f_0+B/2} |H(f)|^2\,df}{B\sqrt{1+2\displaystyle\sum_{\tau=1}^{N-1}\frac{N-\tau}{N}\frac{R_{tt}^2(\tau)}{R_{tt}^2(0)}}}. \quad (8)$$

For instance, the FIR filter function with bandpass response is generally written as

$$h(i) = w(i)\cdot 2\cos\left[2\pi(i-L)\frac{f_0}{B}\right]\cdot\frac{B_c}{2B}\frac{\sin\left[(i-L)\dfrac{B_c}{2B}\pi\right]}{(i-L)\dfrac{B_c}{2B}\pi}, \quad (9)$$

where B_c is the cut-off frequency of the filter, L is the group delay, and w is the window function to save the Gibb's phenomenon. Under the requirement that the digital filter cuts an 8-MHz bandwidth out of the range of 512 MHz, from equations (6), (8), and (9) by generating the Gaussian random variable, we can derive the relationship between the tap length and the sensitivity loss factor, as shown in figure 3. We decided a tap length of 1024 for the VERA terminal based on a comparison between the material size and the sensitivity loss factor. Thus, using the same method, we can show the relationship between the tap-coefficient word length and the sensitivity loss factor, as shown in figure 4. Finally, we decided the tap-coefficient word length to be 13–14 bits in order to realize the minimum material size and cost in the sense that the sensitivity loss factor is about 0.97 (= 3% loss). The specifications of Digital Filter Units are listed in table 3.

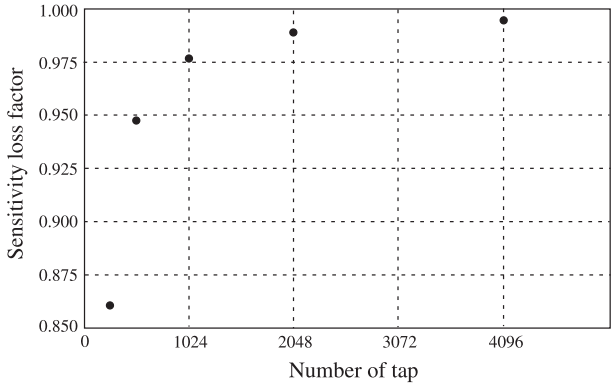

Fig. 3. Relationship between the tap length and the sensitivity loss factor. The results were obtained from the FIR filter in which B_c was equal to B and the Hanning window function was used.

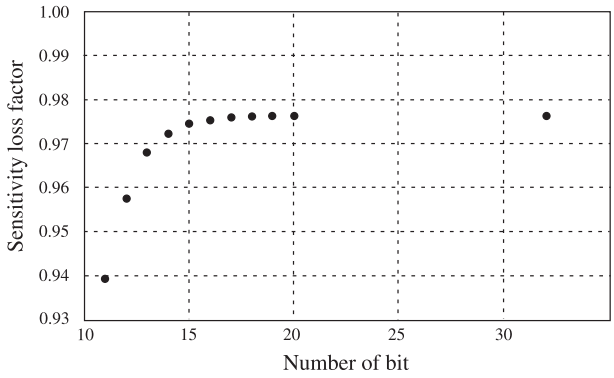

Fig. 4. Relationship between the tap-coefficient word length and the sensitivity loss factor. The results were obtained from the FIR filter with a tap length of 1024.

Table 3. Specifications of the Digital Filter Unit.

Minimum bandwidth	8 MHz in 512 MHz
Number of tap	1024
Tap-coefficient word length	13–14 bits
Performance at 8 MHz in 512 MHz	
Sensitivity loss factor in SNR	0.97
Loss	3%

3.2. Logic of the FIR Filter

From the decimation factor of 32 in the Digital Filter Unit, equation (6) is written as

$$t(n) = \sum_{k=0}^{31}\sum_{j=0}^{K/32-1} h(32j+k) * s[n-(32j+k)], \quad (10)$$

where $i = 32j + k$. According to an arbitrary $k(=c)$, the summation of equation (10) is replaced as

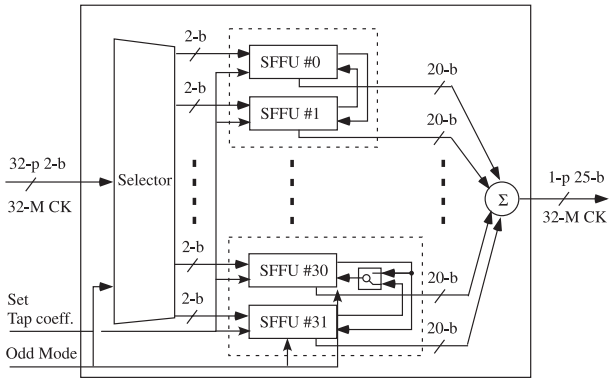

Fig. 5. Block diagram of 32-parallel processing of a FIR filter. The input signals are 32-p 2-bit 32-M CLK, while the output signals are 1-p 25-bit 32-M CLK. The beam selection is done at the last stage, the Input Phase Selector, and the requantization to 2 bits is done at the next stage, the Quantizer (see figure 1). The selector and a switch can change over between an odd tap length or an even one. The SFFU is shown in figure 6.

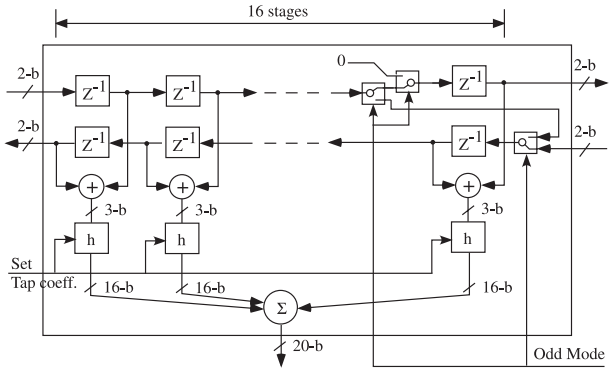

Fig. 6. Block diagram of the Symmetric FIR Filter Unit (SFFU). One SFFU is a 32-tap FIR filter, and has a 7-level look-up table represented by a 16-bit word length as multiplying the tap-coefficient word length by the result after adding the signal and returned one. The output bit length becomes 20 bits [16 bits + $\log_2 16$ (stages) bits]. The switch changes over between an odd tap length or an even one.

$$\sum h(32j + c) * s[n - (32j + c)] = \sum h(l) * s(n - l), \quad (11)$$

where $32j + c = l$, and shows the same equation as equation (6), although its tap length becomes $K/32$. These results imply that the 1024-tap FIR filter consists of 32-parallel independent digital filters with tap coefficients corresponding to each other of $h(32j + c)$. In equation (6), $t(n)$ is calculated from $s(n)$ to $s(n - K + 1)$ with the K continuous samples, and is expressed as follows:

$$\begin{aligned} t(n) &\leqq s(n), \quad s(n-1), \cdots, s(n-K+1), \\ t(n+1) &\leqq s(n+1), s(n), \quad \cdots, s(n-K+2), \\ t(n+2) &\leqq s(n+2), s(n+1), \cdots, s(n-K+3), \end{aligned} \quad (12)$$

However, since the down sampling of $1/32$ is realized by choosing $t(n)$ every 32 samples, the data from $t(n + 1)$ to $t(n + 31)$ are negligible, or thrown out. Thus, equation (10) is rewritten as

$$t(32m) = \sum_{k=0}^{31} \sum_{j=0}^{K/32-1} h(32j + k) * s[32m - (32j + k)], \quad (13)$$

where $n = 32m$.

The FIR filter function with the even symmetrical response, in case that the number of tap is even, has the following relation:

$$h(K - 1 - i) = h(i). \quad (14)$$

Then, equation (13) of a FIR filter is replaced by

$$\begin{aligned} t(32m) = \sum_{k=0}^{31} \sum_{j=0}^{K/64-1} & h(32j + k) * [s(32m - 32j - k) \\ & + s(32m - K + 32j + k + 1)]. \end{aligned} \quad (15)$$

A block diagram with such an algorithm is shown in figure 5. The first summation composes the 32-parallel processing, and second summation does the Symmetric FIR Filter Unit (SFFU), as shown in figure 6. The 16-bit word length after multiplying enables us to understand that a tap-coefficient word length of more than 13 bits is achieved in this design, because 3-bit outputs from the adder circuits after shifting are not represented by 8 levels, but 7 ones.

3.3. Custom FIR Filter Chip and Digital Filter Unit Board

The Digital Filter Unit with 1024 taps consists of four custom FIR filter chips, made of the "Application Specific Integrated Circuit (ASIC)" (see figure 7). The custom FIR filter chip is the SLA50000H series (SLA550QH) with the LSI package of QFP8-208 pin, 0.35 μm silicon gate CMOS using a 4-layer Al interconnect process made by Seiko Epson Corporation. The operating voltage is 3.3 ± 0.3 V at I/O, and 2.0 ± 0.2 V at internal logic, while the operating ambient temperature is 0 to 70°C at a wind speed of 0 m s^{-1}. The eight SFFUs (see figure 6) are packed into a custom FIR filter chip that has a capability of 256 taps. Then, the output bit length from the FIR filter chip becomes 23 bits (20 bit + $\log_2 8$). In addition, the function of the bit distribution measurement is implemented in the FIR filter chip to maximize the performance of digital filtering. The electric power consumption is 420 mW at 3.3 (V), and 620 mW at 2.0 (V).

As shown in figure 8, the Digital Filter Unit board consists of two Digital Filter Units; eight custom FIR filter chips; three Field Programmable Gate Arrays (FPGA), which are ACEX series 1K30 made of ALTERA Corporation; and a 3.3 V onboard power supply. The merit of this structure is that the board size is minimized by being able to implement each quantization function in one FPGA. The Input Phase Selector is made of one FPGA, the 1024-tap FIR filter is made of four custom FIR filter chips, and two Quantizers are included in the last FPGA. A single-phase DC-DC power module is the RM100-48-3.3, made by Densei-Lambda K.K., which converts 48 V to 3.3 V with the maximum output power of 66 W at 86% efficiency. The nominal output power is 38.8 W, which corresponds to a 59% load.

3.4. The GDFB

The GDFB module board placement is shown in figure 9. The filter module consists of one Monitor & Control Unit

Fig. 7. Photograph of the custom FIR filter chip.

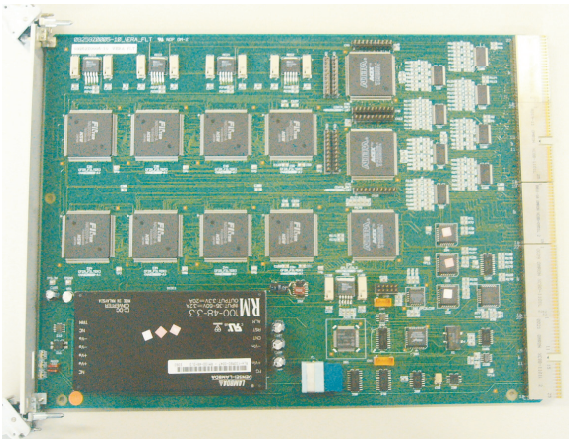

Fig. 8. Photograph of the Digital Filter Unit board. The size is (W) 310 mm × (D) 233.33 mm.

board, one Input I/F Unit board, one data-throughout board, two Power Supply boards, eight Digital Filter Unit boards, and one filter output board. The output module consists of one filter input board, one VSI-H interface board, one VSOP/K-4 interface board, one DSD interface board, one Power Supply board, 16 control keys, and a monitor and control panel, which has status alarms, a reset switch, a time-display LED (Light-Emitting Diode), and a LCD (Liquid Crystal Display) to monitor and control.

The connector specifications of input/output are MDR-68 pin (ECL level), MDR-80 pin and MDR-14 pin [LVDS (Low Voltage Differential Signaling) level], DSUB-25 pin (ECL level), DHA-50 pin (ECL level), FC-10 pin (RS485 level), BNC (ECL level), and BNC (TTL level). Four MDR-68 pin connectors receive data streams from two ADCs, and others transmit them to the PCD. One MDR-14 pin connector receives the IRIG-B signal, 1 PPS and 32-MHz clock; the other MDR-14 pin connector transmits the VSI time code to the VERA recording system. The ECL-level BNC connector transmits Start signal to the RVC, and the TTL-level BNC connectors transmit 1 PPS to the VSOP recorder and Start signal to the DSD. The MDR-80 pin connector transmits the VSI-H specification data streams to the VERA recording system, the DSUB-25 pin connector transmits the VSOP/K4 data streams to the VSOP recorder and the RVC, and the DHA-50 pin connector transmits the DSD data streams to the DSD.

The power consumption of the filter module is 610 W, while that of the output module is 140 W. The total AC power is 750 W at 1-phase 100 VAC 50/60 Hz. The total weight of the GDFB is 63.4 kg.

A summary of GFDB key specifications is given in table 4.

4. Performance and Demonstration

This section shows the evaluation results of the VERA digital backend subsystem, the GDFB, in the VERA terminal. We present the simulation results to estimate the digital loss factor, including the requantization process after digital filtering (see subsection 4.1) and the measurement results of the VERA GDFB frequency response, to deeply investigate the stopband and sharpness of the digital filter after requantizing (see subsection 4.2). They also demonstrate the VERA observations with GDFBs to verify the astronomical GDFB response (see subsection 4.3). We further discuss the bandedge and folding noise of the digital filter (see subsection 4.4).

4.1. Digital Loss Factor

The astronomical analog waveforms are sampled by ADCs with 4-level (2-bit) quantization in the VERA system. The GDFB cuts the requested frequency bands in the digital waveforms with 4-level quantized sampling. The digital waveform after digital filtering is represented by multi-level quantized sampling in the calculation process of the digital filter, as shown in equation (6). It thus requires requantization after digital filtering, because the recording data rate, the digital data transmission rate or the data processing rate is limited by the instrumental capability. The quantization noise in digitizing has been investigated on a theoretical basis (Thompson et al. 2001; Iguchi, Kawaguchi 2002). It is well known that the digital loss factor becomes 0.64 at the 2-level (1-bit) quantization loss factor and 0.88 at the 4-level quantization loss factor. However, the digital noise effect by the requantization process had been unknown in cases of input and output waveforms with 2- or 4-level quantized sampling. This paper presents the results that a computer simulation was run to investigate the digital loss factor, including the requantization process after digital filtering the digital waveforms with 4-level quantized sampling. In this simulation, the 1/4-bandpass digital filter with 1024 taps was used to diminish the effect of the digital filter bandpass response. This is much more than those of the GDFB, a 1/64-bandpass digital filter (= 8 MHz/512 MHz) with 1024 taps (see table 3), and thus corresponds to the 8192 taps in the GDFB.

The *SNR* on correlation with unquantized sampling can be written simply as

$$SNR = \frac{R_{xy}(0)}{\sqrt{R_{xx}(0)R_{yy}(0) + R_{xy}^2(0)}}\sqrt{N}$$

$$= \frac{\rho}{\sqrt{1+\rho^2}}\sqrt{N}, \qquad (16)$$

where R_{xy} is the cross-correlation function between x and

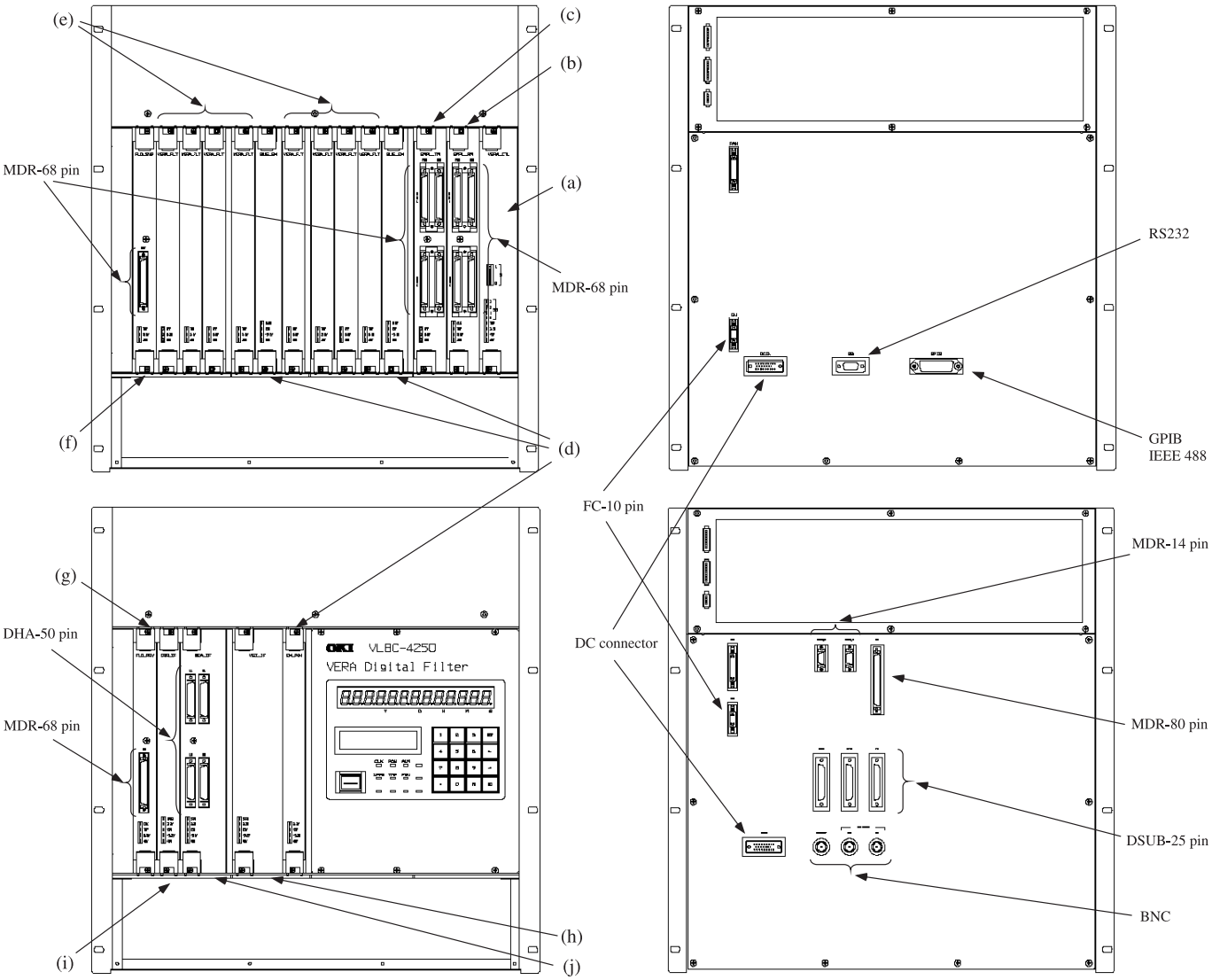

Fig. 9. GDFB board placement. There are two modules: one is the filter module (top: left is front view, and right is back view), having a size of (W) 490 mm × (H) 500 mm × (D) 500 mm; the other one is the output module (bottom: left is front view, and right is back view), having a size of (W) 490 mm × (H) 500 mm × (D)500 mm. Referring to figure 1, (a) is the Monitor & Control Unit board, (b) is the Input I/F Unit board, (c) is the data throughout board for the PCD, (d) is the Power Supply board, (e) is the Digital Filter Unit board, (f) is the filter output board from sixteen Digital Filter Units, (g) is the filter input board from the filter module, (h) is the VSI-H interface board, (i) is the VSOP/K-4 interface board, and (j) is the DSD interface board. The distribution of input signals to sixteen Digital Filter Units is done in the back-panel. The Output I/F Unit is implemented in the output module, and consists of (g), (h), (i), and (j). The total size of the GDFB is (W) 490 mm × (H) 1100 mm × (D) 500 mm, including the power supply module.

y, R_{xx} and R_{yy} are the autocorrelation functions of x and y, respectively, ρ is the correlation coefficient, and N is the number of samples with the Nyquist rate. To estimate the loss within 1% of the true value, SNR must be more than 100. In this simulation, a correlation coefficient of 0.109 $\left[= 0.35^2/\sqrt{(1^2 + 0.35^2)^2}\right]$ when the common/independence component in x and y is 0.35, and N of 1048576 are used to achieve SNR of 111 from the following two conditions: (1) The most correlation coefficient must be less than 0.1 for very small flux densities of cosmic radio sources. (2) Since the astronomical signal waveforms obey the zero-mean Gaussian random variable, it is difficult to provide long-series Gaussian noise data points.

The simulation results are listed in table 5. From a comparison of the theoretical estimations with the simulation results in 2-level and 4-level quantizations, it has been confirmed that a simulation measurement with 1% precision could be achieved. If the requantization process had a linear response, the digital loss factor would be 0.56 (= $0.881 * 0.637$) and 0.78 (= $0.881 * 0.881$) at the 2-level and 4-level requantizations after digital by filtering the digital waveforms with 4-level quantized sampling, respectively. However, the simulation results show digital loss factors of 0.59 and 0.81 (see table 5). This means that the requantization process of the input and output waveforms with 2- or 4-level quantized sampling has a nonlinear response. The least significant bit (LSB) has

Table 4. The specifications of Gigabit Digital Filter Bank.

Configuration:	Filter module, Output module, and Power module
Filter module:	16 Digital filter units with 1024 tap lengths
Input data rate:	
ADC:	2048 Mbps × 2 beams
Observation modes:	
	see table 1
Output data rate:	
VERA recorder:	1024, 512, 256 Mbps
VSOP recorder:	256, 128 Mbps
RVC:	256, 128 Mbps
DSD:	1024, 512, 256 Mbps
PCD:	2048 Mbps × 2 beams
Monitor and Control:	
	Control computer controls via GPIB IEEE-488
Dimensions:	(W) (H) (D)
Filter module:	$49 \times 50 \times 50\,\mathrm{cm}^3$
Output module:	$49 \times 50 \times 50\,\mathrm{cm}^3$
Power module:	$49 \times 10 \times 50\,\mathrm{cm}^3$
Total:	$49 \times 110 \times 50\,\mathrm{cm}^3$
Weight:	
Filter module:	28.0 kg
Output module:	22.2 kg
Power module:	13.2 kg
Total:	63.4 kg
Power consumption:	
Filter module:	610 W
Output module:	140 W
Total:	750 W

50% uncertainty, and thus these roundoff errors are accumulated in the calculation process of digital filtering, as shown in equation (6). Although multi-level digital waveforms seem to be approximately equal to the analog waveforms, those digital waveforms have roundoff errors accumulated by the input digital waveforms with a digital loss factor of 0.88. On the other hand, the 2- or 4-level requantization would cut off not only the information of the signal component, but also a part of the effects of roundoff errors and quantization loss. Actually, the digital loss factor of 0.81 agrees completely with that of 3-level (2-bit) quantization (see Thompson et al. 2001). The simulation results show that the digital loss factor is not 0.56, but 0.59, and not 0.78, but 0.81 in 2-level and 4-level requantizations after digital filtering the digital waveforms with 4-level quantized sampling.

4.2. VERA GDFB Frequency Response

Figure 10 shows a block diagram of the measurement setup of the GDFB frequency response. To investigate the frequency response, it is useful to use the CW signal, which can measure

Table 5. Simulation results of the digital loss factor.*

Quantization	Requantization	Digital loss factor	
		Theory	Simulation
2 levels	···	0.64	0.64 ± 0.01
4 levels	···	0.88	0.88 ± 0.01
4 levels	2 levels		0.59 ± 0.01
4 levels	4 levels		0.81 ± 0.01

* Including the requantization process after digitally filtering the digital waveforms with 4-level quantized sampling, excluding the frequency response of the digital filter.

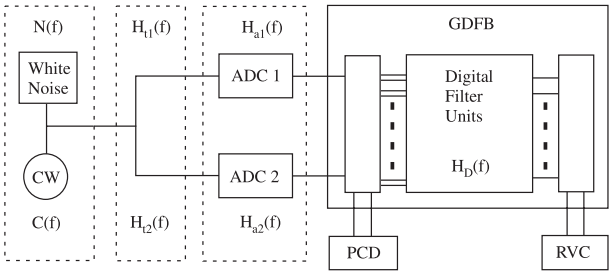

Fig. 10. Block diagram of the measurement setup. A detailed block diagram of GDFB is shown in figure 1. The white noise is derived from the VERA analog backend subsystem, while the CW signal is produced by the Agilent E4423B, which is locked in phase to a standard signal of 10 MHz generated by the master oscillator. The ADC 1 and ADC 2 with 1024 Msps are locked to the same standard signal of 10 MHz. Note that the ADS-1000 made by Digital Link Company, the next generation VERA ADC, was used as the ADCs in this measurement.

the folding effects by sweeping the frequency range of 0 to 512 MHz. The white noise is important to measure the frequency response, because the astronomical signals obey the Gaussian random variable. To approximate the zero-mean Gaussian probability, the input signals are a combination of both the CW signal and the white noise.

The frequency response before digital filtering is obtained with the PCD, and is written as

$$P^{\mathrm{I}}_{\mathrm{on}}(f) = \left[|C(f)|^2 + |N(f)|^2\right] \cdot H_1(f)H_2^*(f), \tag{17}$$

where $C(f)$ is the frequency response of the CW signal, $N(f)$ is the frequency response of the white noise from the VERA analog backend subsystem, and H_1 and H_2 are the frequency response by different transmission paths, in which $H_1 = H_{\mathrm{t1}}H_{\mathrm{a1}}$ and $H_2 = H_{\mathrm{t2}}H_{\mathrm{a2}}$ (see figure 10). The bandpass calibration is essential for estimating the precise CW power, because the bandpass response becomes a time-variable due to the outdoor air temperature. The frequency response without the CW signal is written as

$$P^{\mathrm{I}}_{\mathrm{off}}(f) = |N(f)|^2 \cdot H_1(f)H_2^*(f). \tag{18}$$

Finally, the CW frequency response including the response of measurement system is derived as

$$P^{\mathrm{I}}(f) = P^{\mathrm{I}}_{\mathrm{on}} - P^{\mathrm{I}}_{\mathrm{off}} = |C(f)|^2 \cdot H_1(f)H_2^*(f). \tag{19}$$

The frequency response after digital filtering, down

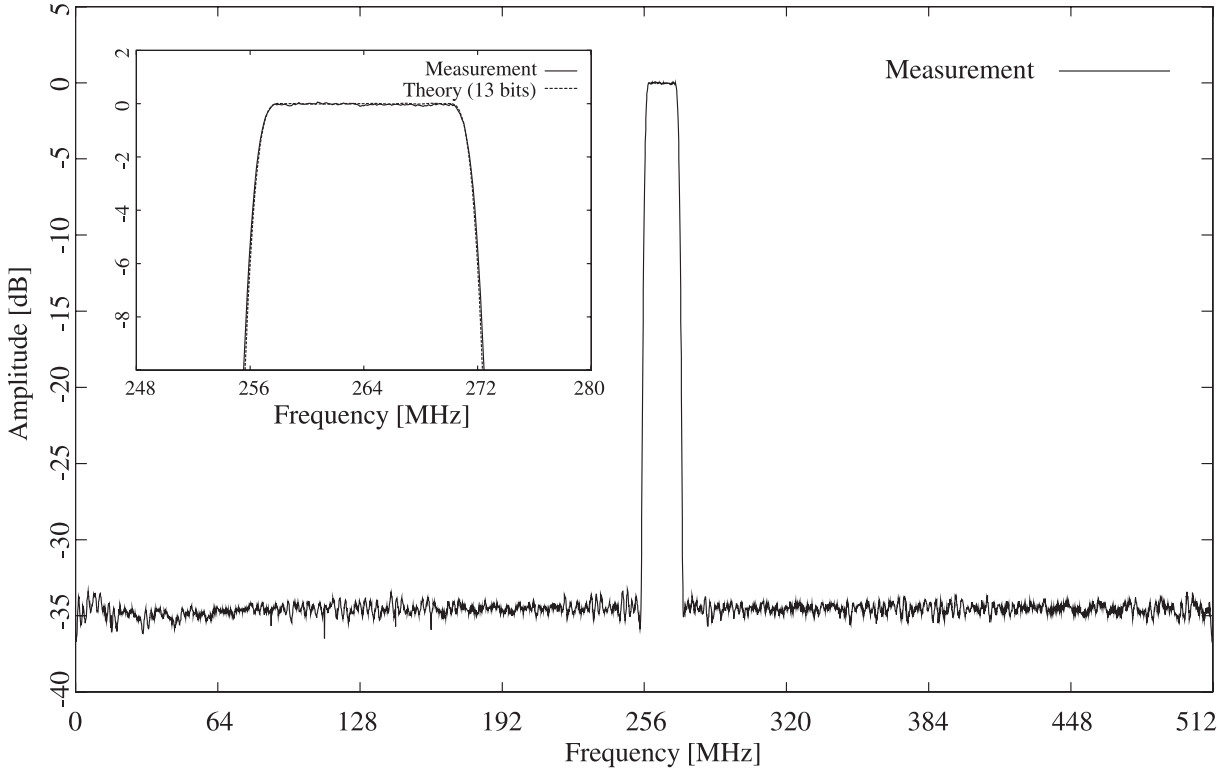

Fig. 11. Measured VERA GDFB response at a bandwidth of 16 MHz in a frequency rage of 256 to 272 MHz with a tap length of 1024. A stopband response of about −35 dB was successfully achieved. A comparison between the measured frequency response of VERA GDFB (full line) and the ideal frequency response of FIR filter at 13 bits (dotted line) is shown in a sub-panel. The passband response was −5.3 dB at the bandedges of 256 and 272 MHz, but the design value was just −6 dB.

sampling and requantization in the GDFB is measured with the RVC (Iguchi et al. 2000b), and is written as

$$P^{\mathrm{O}}_{\mathrm{on}}(f) = \left[|C(f)|^2 + |N(f)|^2\right] \cdot H_1(f)H_2^*(f) \cdot |H_{\mathrm{D}}(f)|^2, \tag{20}$$

where H_{D} is the VERA GDFB frequency response, including the effects of requantization and the folding noise after down sampling. The frequency response without the CW signal can be written as

$$P^{\mathrm{O}}_{\mathrm{off}}(f) = |N(f)|^2 \cdot H_1(f)H_2^*(f) \cdot |H_{\mathrm{D}}(f)|^2, \tag{21}$$

and then the CW frequency response including the response of measurement system is derived as

$$\begin{aligned} P^{\mathrm{O}}(f) &= P^{\mathrm{O}}_{\mathrm{on}} - P^{\mathrm{O}}_{\mathrm{off}} \\ &= |C(f)|^2 \cdot H_1(f)H_2^*(f) \cdot |H_{\mathrm{D}}(f)|^2. \end{aligned} \tag{22}$$

From equations (19) and (22), we can derive the VERA GDFB frequency response from the correlated spectra obtained by both the PCD and the RVC as

$$|H_{\mathrm{D}}|^2 = \frac{P^{\mathrm{O}}(f)}{P^{\mathrm{I}}(f)}. \tag{23}$$

To derive $P^{\mathrm{O}}(f)$ precisely, we need to carefully adjust the CW power in the measurement. The power of CW signals from 0 to 512 MHz has to be decided by the relative power of the CW signal to the white noise. When the power of the CW signal is 1000 times stronger than (up 30 dB) the continuum floor level of the white noise spectrum, 2-bit ADCs will work as 1-bit performance. In that case, it is important to adjust the power as studiously as possible while avoiding the high-order spurious effects. The frequency responses of $P_{\mathrm{on}}(f)$ and $P_{\mathrm{off}}(f)$ must also be varied delicately with the relative power of CW signal to the white noise, and also the threshold levels in quantization and requantization. To correct this effect, we need to calibrate the bandpass by sensitively adjusting the continuum floor level of P_{off} to that of P_{on} in the data analysis.

Figure 11 shows the VERA GDFB frequency response at a bandwidth of 16 MHz in the range of 256 to 272 MHz. Measurements without the CW signal for the bandpass calibration were made every 30 minutes. The measurement frequency resolution was 125 kHz. The measurement results show the effective bandwidth of 15.14 MHz, which was obtained by passband responses of −1 dB at 256.8 and 271.2 MHz, −3 dB at 256.3 and 271.7 MHz, and −5.3 dB at bandedges of 256 and 272 MHz, and realized by a stopband response of about −35 dB. However, the design value with a gain of −6 dB at the bandedges and an out-of-band stopband response of less than −60 dB have been expected in the case of a tap-coefficient word length of 13 bits. This problem is likely to be due to the rounding errors in the calculation process and the requantization after digital filtering. A deeper discussion will be reported by Kurayama and Iguchi (in preparation), adding the measurement results of several output bandwidths.

4.3. Astronomical Demonstrations

The VERA-7 observation mode, which is 16-IFch 16-MHz bandwidth at 2-bit quantization (see table 1), was tested with VERA. The celestial radio source pairs, W 3 OH (Beam 1) and J0244+6228 (Beam 2) with its separation of 2°17, and J1424+0434 (Beam 1) and 3C 273B (Beam 2) with its separation of 1°80, was observed at 22.22700781 (Beam 1) and 22.09911719 GHz (Beam 2) on 2003 December 23, respectively, on a baseline between the VERA IRIKI 20-m and VERA ISHIGAKI 20-m radio telescopes. We sorted W 3 OH into one IF channel only and J0244+6228 into fifteen IF channels, while we sorted J1424+0434 into one IF channel only and 3C 273B into fifteen IF channels. The observed data were cross-correlated with the VSOP correlator modifying for the VERA (Kobayashi et al. 2003). A fringe fitting was made using the NRAO AIPS package. We used solution intervals of 2 minutes for J0244+6228 and of 1 minutes for the others, and accepted all solutions with $SNR > 7$. After a radio interferometric correlation without any bandpass calibrations, the cross-power spectra of each pair are shown in figures 12 and 13. The amplitude (at scalar) and phase (at vector) were integrated at an interval time of 120 seconds for W 3 OH and at an interval time of 300 seconds for the others. Note that these spectra were obtained without the correction of the different amplitude intensities between the IFs or bands.

Figure 12 shows the H_2O maser emissions from W 3 OH (Beam 1) and the continuum emissions from J0244+6228 (Beam 2). The spectrum in W 3 OH was smoothed to 512 frequency channels in the frequency range of 16 MHz (IF 1), while the spectrum in J0244+6228 was smoothed to 15 frequency channels in the frequency range of 240 MHz, which consists of fifteen IF channels of 16-MHz bandwidth (IF 2-16). The effective bandwidth in the frequency range of 240 MHz becomes 227 MHz. This IF configuration will be well used and operated in the VERA project, which enables us to observe a galactic maser source and a nearby reference source simultaneously. The results of the first dual-beam observations with our developed VERA GDFB were presented by Honma et al. (2003), demonstrating that the atmospheric phase fluctuation was effectively removed by dual-beam phase referencing.

Figure 13 shows the continuum emissions from J1424+0434 (Beam 1) and 3C 273B (Beam 2). All IFs were smoothed to 32 frequency channels in the frequency range of 16 MHz. The spectra in J1424+0434 has 32 frequency channels in the frequency range of 16 MHz (IF 1), while the spectra in 3C 273B has 480 frequency channels in the frequency range of 240 MHz, which consists of fifteen IF channels of 16-MHz bandwidth (IF 2-16). The average of each IF's effective bandwidth in 3C 273B is 15.1 MHz, and the total effective bandwidth becomes 227 MHz. Since these results correspond with that of J0244+6228 completely, it's not difficult to understand that the effective bandwidth strongly depends on the digital filter response with the slope response at the bandedge. This IF configuration is available and effective in the high-precision astrometric observation toward investigating the motion and position of radio sources; e.g. the detection of the Kepler orbital motion of some emission component close to black holes (Sudou et al. 2003).

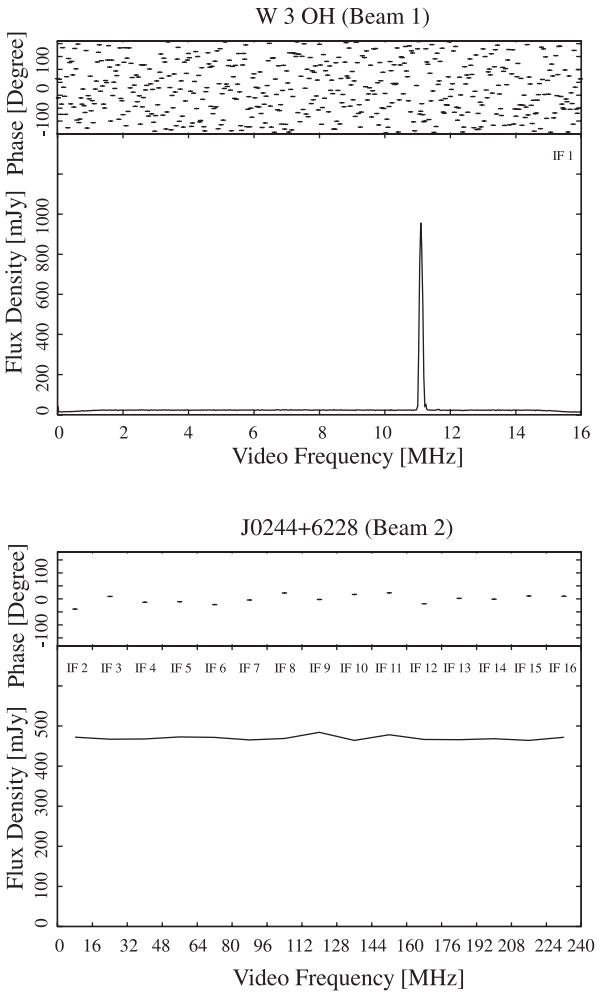

Fig. 12. Phase and amplitude responses of the cross-power spectrum in W 3 OH at 22.22700781 GHz (Beam 1) and J0244+6228 at 22.09911719 GHz (Beam 2) on a baseline between the VERA ISHIGAKI and VERA IRIKI telescopes. The amplitude (at scalar) and phase (at vector) are integrated at an interval time of 120 seconds for W 3 OH and at an interval time of 300 seconds for J0244+6228. The observation mode is 16-IFch 16-MHz bandwidth at 2-bit quantization, VERA-7 (see table 1). W 3 OH was allocated to one IF channel only, while J0244+6228 was allocated to fifteen IF channels. The top panel is the cross-power spectrum of a H_2O maser in W 3 OH with one IF channel of 16-MHz bandwidth (IF 1) with Beam 1. The bottom panel is the cross-power spectrum of the continuum emission in J0244+6228 with fifteen IF channels of 16-MHz bandwidth (IF 2-16) with Beam 2. The W 3 OH spectrum is smoothed to 512 frequency channels in the frequency range of 16 MHz, while J0244+6228 spectrum is smoothed to 15 frequency channels in the frequency range of 240 MHz, which is equal to 15-IFch 16-MHz bandwidth.

4.4. Bandedge and Folding Noise

The filter bank has two big problems: one is a reduction in the effective bandwidth by avoiding the slope response at the bandedge; the other is detection of leakage emission in one IF by folding or aliasing the astronomical signals from the next IFs if powerfully strong sources are observed at the bandedge of the next IFs. However, the folding noise due to aliasing or foldover of noise from frequencies above the

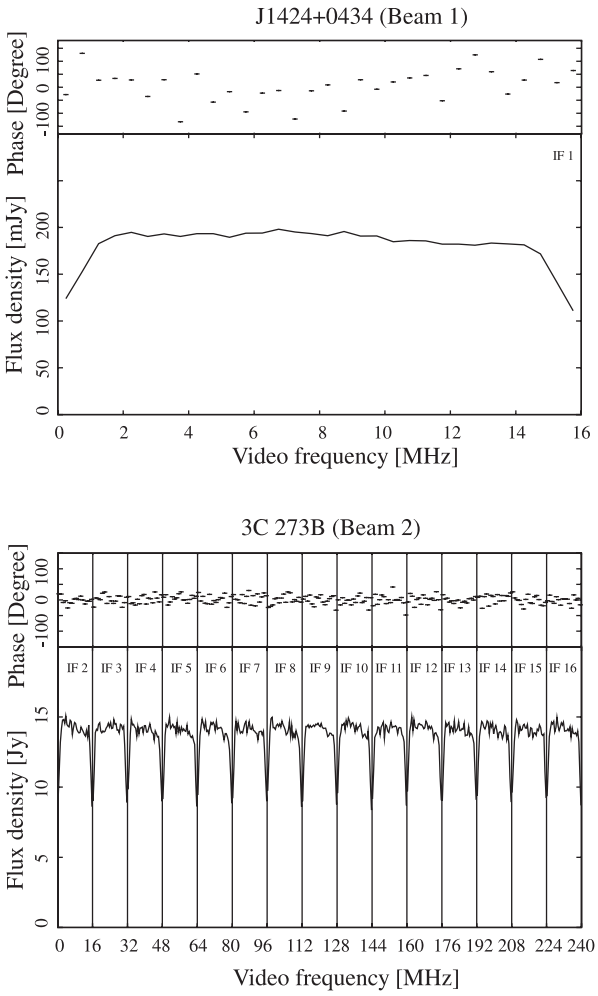

Fig. 13. Phase and amplitude responses of the cross-power spectrum in J1424+0434 at 22.22700781 GHz (Beam 1) and 3C 273B at 22.09911719 GHz (Beam 2) on a baseline between VERA ISHIGAKI and VERA IRIKI telescopes. The amplitude (at scalar) and phase (at vector) were integrated at the interval time of 300 seconds. The observation mode is 16-IFch 16-MHz bandwidth at 2-bit quantization, VERA-7 (see table 1). J1424+0434 was allocated to one IF channel only, while 3C 273B was done to fifteen IF channels. All IFs were smoothed to 32 frequency channels in the frequency range of 16 MHz. The top panel is the cross-power spectrum of continuum emission from J1424+0434 with one IF channel of 16-MHz bandwidth (IF 1) with Beam 1. The bottom panel is the cross-power spectrum of continuum emission from 3C 273B with fifteen IF channels of 16-MHz bandwidth (IF 2-16) with Beam 2.

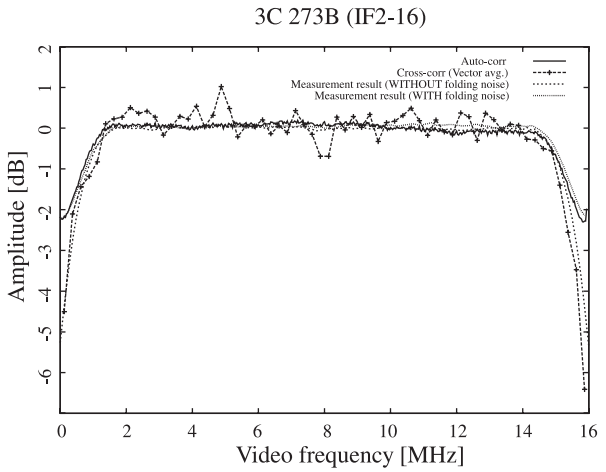

Fig. 14. Comparison between the actual measurement value of the bandpass responses (see figure 11) and the observed cross-power (cross-corr) and power (auto-corr) spectra of 3C 273B (as obtained by integrating the bandpass responses from IF 2 to IF 16, shown in figure 13). These amplitudes, however, were integrated at vector. The cross-power spectrum has 64 channels, while the power spectrum has 512 channels. The auto-correlation and cross-correlation spectra is consistent with the measured GDFB frequency response with the effect of the folding noise and without, respectively.

bandedge is reduced in the phase-rotation process with a high fringe frequency. An astronomical demonstration was reported by Iguchi et al. (2000a). Figure 14 shows that a decrease in the folding noise is accomplished by the VLBI correction process of the geometrical delay variation due to the earth's rotation. The suppression ratio of the folding noise at an integration interval of 1 seconds becomes less than -45 dB $[-10\log(1/2\pi f_r)]$, for which the fringe frequency (f_r) is about 5 kHz at 22 GHz with a projected baseline length of about 1000 km, which is shortest distance in VERA, given that these big problems become vanishingly small.

5. Conclusion and Future Prospects

We have successfully developed GDFBs that are implemented as the VERA digital backend subsystem in the VERA terminal, demonstrating that the realization of a stopband response of about -35 dB is technically feasible in the case of a 16-MHz output bandwidth. The GDFB consists of sixteen Digital Filter Units with 1024 tap lengths. The GDFB can easily give us an arrangement having a flexible bandwidth within the sampling frequency. In addition, our developed custom FIR filter chip has a function that the bit distribution after digital filtering is measured, giving the optimum threshold level for maximizing the sensitivity in sampling with ADC.

We have successfully obtained the first astronomical fringe spectrum of GDFBs, demonstrating that the realization of dual-beam differential VLBI is technically feasible. The GDFB can choose the output channels to observe two adjacent sources simultaneously, giving the position of a galactic maser relative to an extra-galactic reference source with unprecedentedly high accuracy.

We have installed the new digital backend system with our developed custom FIR filter chips in the BEARS (BEam Array Receiver System), which is a multi-beam system with an array receiver of 25 elements implemented in the 45-m telescope at Nobeyama Radio Observatory (Iguchi et al. 2003). The BEARS has the requirement that a digital filter with 512 taps cuts a 16-MHz bandwidth out of the range of 512 MHz, while one with 256 taps does a 32-MHz bandwidth.

We are improving the our GDFB for the Korean VLBI Network (KVN), which is a project to construct a millimeter-wave VLBI network to mainly research the interstellar molecular cloud for the first scientific targets (Minh et al. 2003). The KVN is going to employ a multi-frequency band receiver

system to calibrate the phase for millimeter-wave VLBI. The KVN Data Acquisition System (KVNDAS) needs four ADCs to meet the requirement. We can meet the KVNDAS specifications by introducing a few minor changes in the interface of GDFB, which changes two input ports into four.

The new XF architecture with digital filter banks, the Digital Hybrid XF correlator, was proposed, and has been developed for the next-generation radio interferometers, e.g. the Expanded Very Large Array (EVLA) and the Atacama Large Millimeter/submillimeter Array (ALMA). The design and development of digital filter banks for ELVA and ALMA have been deeply examined by Carlson (2001), Escoffier and Webber (2002), and Quertier et al. (2003). We successfully measured the performances of the digital filter, and demonstrated the capability of a wide-frequency coverage and high-frequency resolution of the correlation systems for an interferometer. Our development and measurement results will also be useful and helpful in designing and developing the digital filter of the Digital Hybrid XF correlator.

References

Carlson, B. 2001, NRC-EVLA Memo 014 (Victoria: NRC; Charlottesville: NRAO)

Escoffier, R., & Webber, J. 2002, ALMA Memo 441 (Charlottesville: NRAO)

Honma, M., et al. 2003, PASJ, 55, L57

Honma, M., Kawaguchi, N., & Sasao, T. 2000, in Proc. SPIE 4015, Radio Telescope, ed. H. R. Butcher, 624

Iguchi, S., & Kawaguchi, N. 2002, Institute of the Electronics, Information and Commication Engineers (IEICE) Trans. Commun., E85-B, 9, 266

Iguchi, S., Kawaguchi, N., Kameno, S., Kobayashi, H., & Kiuchi, H. 2000a, IEICE Trans. Commun., E83-B, 2, 406

Iguchi, S., Kawaguchi, N., Murata, Y., Kobayashi, H., Fujisawa, K., & Miki, T. 2000b, IEICE Trans. Commun., E83-B, 11, 2527

Iguchi, S., Kawaguchi, N, Okumura, S. K., & Sunada, K. 2003, in ASP Conf. Ser., 306, New Technologies in VLBI, ed. Y. C. Minh, 161

Kawaguchi, N., Sasao, T., & Manabe, S. 2000, in Proc. SPIE 4015, Radio Telescope, ed. H. R. Butcher, 544

Kiuchi, H., Amagai, J., Hama, S., & Imae, M. 1997, PASJ, 49, 699

Kobayashi, H., et al. 2003, in ASP Conf. Ser., 306, New Technologies in VLBI, ed. Y. C. Minh (San Francisco: ASP), 367

Minh, Y. C., Roh, D.-G., Han, S.-T., & Kim, H.-G. 2003, in ASP Conf. Ser., 306, New Technologies in VLBI, ed. Y. C. Minh, 373

Napier, P. J., Bagri, D. S., Clark, B. G., Rogers, A. E. E., Romney, J. D., Thompson, A. R., & Walker, R. C. 1994, IEEE, 82, 658

Quertier, B., Comoretto, G., Baudry, A., Gunst, A., & Bos, A. 2003, ALMA Memo 476

Sasao, T. 1996, in Proc. 4th Asia-Pacific Telescope (APT) Workshop, ed. E. A. King (Sydney: ATNF), 94

Sorai, K., Sunada, K., Okumura, S. K., Iwasa, T., Tanaka, A., Natori, K., & Onuki, H. 2000, in Proc. SPIE, 4015, 86

Sudou, H., Iguchi, S., Murata, Y., & Taniguchi, Y. 2003, Science, 300, 1263

Sunada, K., Yamaguchi, C., Nakai, N., Sorai, K., Okumura, S. K., & Ukita, N. 2000, Proc. SPIE, 4015, 237

Thompson, A. R., Moran, J. M., & Swenson, G. W., Jr. 2001, Interferometry and Synthesis in Radio Astronomy, 2nd ed., (New York: John Wiley & Sons), 289

Whitney, A. R. 1993, in Developments in Astronomy and Their Impact on Astrophysics and Geodynamics, ed. I. I. Mueller & B. Kolaczek (Dordrecht: Kluwer), 151